Ligand migration and hexacoordination in type 1 non-symbiotic rice hemoglobin

ARTICLE *in* BIOCHIMICA ET BIOPHYSICA ACTA · OCTOBER 2010

Impact Factor: 4.66 · DOI: 10.1016/j.bbapap.2010.09.016 · Source: PubMed

8 AUTHORS, INCLUDING:

Nitin Kumar Bisht
Henry Ford Health System
1 PUBLICATION **8** CITATIONS
SEE PROFILE

Stefania Abbruzzetti
Università degli studi di Parma
75 PUBLICATIONS **1,392** CITATIONS
SEE PROFILE

Stefano Bruno
Università degli studi di Parma
76 PUBLICATIONS **1,198** CITATIONS
SEE PROFILE

Francesca Spyrakis
Università degli Studi di Modena e Reggio E…
61 PUBLICATIONS **1,098** CITATIONS
SEE PROFILE

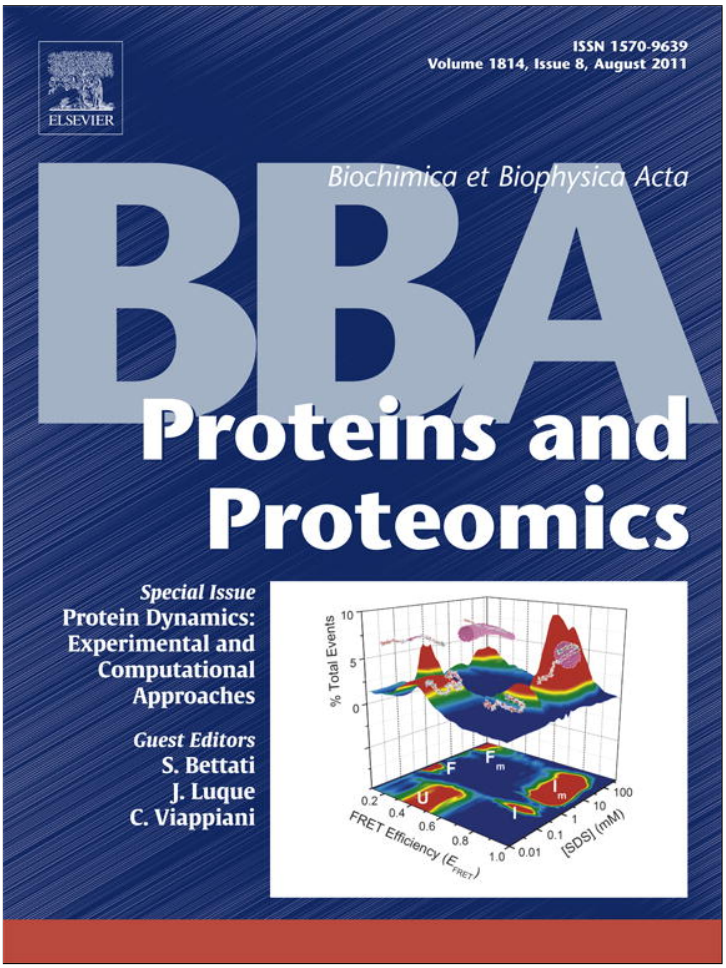

Biochimica et Biophysica Acta 1814 (2011) 1042–1053

Contents lists available at ScienceDirect

Biochimica et Biophysica Acta

journal homepage: www.elsevier.com/locate/bbapap

Ligand migration and hexacoordination in type 1 non-symbiotic rice hemoglobin ☆

Nitin Kumar Bisht [a,b,c], Stefania Abbruzzetti [a,b], Sheetal Uppal [c], Stefano Bruno [d], Francesca Spyrakis [e,f], Andrea Mozzarelli [d,e], Cristiano Viappiani [a,g,*], Suman Kundu [c]

[a] Dipartimento di Fisica, Università degli Studi di Parma, Parma, Italy
[b] Dipartimento di Biotecnologie, Università degli Studi di Verona, Italy
[c] Department of Biochemistry, University of Delhi South Campus, New Delhi, India
[d] Dipartimento di Biochimica e Biologia Molecolare, Università degli Studi di Parma, Parma, Italy
[e] INBB, Biostructures and Biosystems National Institute, Italy
[f] Dipartimento di Chimica Generale ed Inorganica, Chimica Analitica, Chimica Fisica, Università degli Studi di Parma, Italy
[g] NEST, Istituto Nanoscienze-CNR, Italy

ARTICLE INFO

Article history:
Received 29 July 2010
Received in revised form 26 September 2010
Accepted 28 September 2010
Available online 29 October 2010

Keywords:
Non-symbiotic plant hemoglobin
Laser flash photolysis
Silica gel
Ligand migration
Hexacoordination

ABSTRACT

Type 1 non-symbiotic rice hemoglobin (rHb1) shows bis-histidyl heme hexacoordination and is capable of binding diatomic ligands reversibly. The biological function is as yet unclear, but the high oxygen affinity makes it unlikely to be involved in oxygen transport. In order to gain insight into possible physiological roles, we have studied CO rebinding kinetics after laser flash photolysis of rHb1 in solution and encapsulated in silica gel. CO rebinding to wt rHb1 in solution occurs through a fast geminate phase with no sign of rebinding from internal docking sites. Encapsulation in silica gel enhances migration to internal cavities. Site-directed mutagenesis of FB10, a residue known to have a key role in the regulation of hexacoordination and ligand affinity, resulted in substantial effects on the rebinding kinetics, partly inhibiting ligand exit to the solvent, enhancing geminate rebinding and enabling ligand migration within the internal cavities. The mutation of HE7, one of the histidyl residues involved in the hexacoordination, prevents hexacoordination, as expected, but also exposes ligand migration through a complex system of cavities. This article is part of a Special Issue entitled: Protein Dynamics: Experimental and Computational Approaches.

1. Introduction

The presence of hemoglobins (Hbs) in plants is well known since the discovery of leghemoglobins in the nodules of legumes where they transport oxygen to nitrogen-fixing endosymbiotic bacteria [1]. More recently, it was found that plants contain additional classes of hemoglobins, which have been termed non-symbiotic Hbs (nsHbs) since they are not linked to nitrogen-fixing bacteria [2–5]. nsHbs are normally divided into class 1 nsHbs, characterized by a very high oxygen affinity, and class 2 nsHbs, which have lower affinity for oxygen. A third class of nsHbs found in plants has some structural features resembling bacterial truncated Hbs [6–8]. The functions and mechanisms of regulation of ligand binding of nsHbs are a current subject of vigorous investigation. The three major phylogenetically distinct nsHb genes are individually regulated and almost certainly have distinct functions [8].

Type 1 nsHbs are upregulated under hypoxia, osmotic stress, nutrient deprivation, cold stress, rhizobial infection, nitric oxide exposure, and fungal infection and may represent some of the defense strategies against stress with as yet partly unknown mechanisms [4,7,9,10]. There is consensus about the involvement of type 1 nsHbs in a metabolic pathway involving NO, which may provide an alternative type of respiration to mitochondrial electron transport under limiting oxygen concentrations [7]. It was suggested that type 1 nsHbs under hypoxic conditions act as part of a soluble, terminal, NO dioxygenase system, yielding nitrate from the reaction of oxyHb with NO [11]. The overall reaction consumes NADH and maintains ATP levels via an as yet unknown mechanism.

Type 1 nsHb from *Arabidopsis thaliana* (AHb1) was indeed shown to have a NO dioxygenase activity *in vitro*, which may reduce levels of NO under hypoxic stress [12]. Biochemical evidence indicates that rapid nitrate accumulation is accompanied by NO-dependent oxidation of oxygenated to oxidized AHb1. The Fe^{3+} heme can be directly reduced by NADPH, which supports continuous nitrate accumulation in the presence of excess NO. Otherwise, oxidized nsHb might be reduced by a mixture of NADH and FAD, or by a methemoglobin reductase [13]. NO dioxygease activity *in vitro* was recently studied in detail for type 1 nsHb from rice (rHb1) [11] and from barley [14].

A striking feature of non-symbiotic Hbs is hexacoordination of the heme iron through interactions with HisE7 and HisF8 in the absence of exogenous ligands. In spite of hexacoordination, oxygen affinity of

☆ This article is part of a Special Issue entitled: Protein Dynamics: Experimental and Computational Approaches.

* Corresponding author. Dipartimento di Fisica, Università degli Studi di Parma, Parma, Italy. Tel.: +39 0521905208; fax: +39 0521905223.
E-mail address: cristiano.viappiani@fis.unipr.it (C. Viappiani).

1570-9639/$ – see front matter © 2010 Elsevier B.V. All rights reserved.
doi:10.1016/j.bbapap.2010.09.016

these proteins is very high (the oxygen dissociation constant K_d is in the submicromolar range), making them unlikely to be involved in oxygen transport [3,4].

Type 1 nsHbs are only weakly hexacoordinated [8,15,16]. Phenylalanine at position B10 is a key regulatory amino acid in the bis-histidyl hexacoordination and it was recently shown for type 1 rice nsHb (rHb1) to be the only amino acid that stabilizes oxygen binding to the ferrous form [16]. In addition, FB10 was shown to be a key element in preventing autoxidation for both rHb1 [16] and AHb1 [17].

Switching from the hexacoordinated to the oxygenated species may be instrumental in sustaining the proposed NO dioxygenase mechanism, as suggested for neuroglobin [18,19]. The sequential NO dioxygenase reaction implies the coexistence of reactive ligand species within the protein matrix, transiently located at secondary binding sites within the protein matrix. Indeed, computational investigations evidenced a system of hydrophobic cavities in *A. thaliana* AHb1, whose connectivity to the heme distal pocket is regulated by hexacoordination [20]. In particular, a tunnel connecting the distal cavity with the solvent becomes available upon distal His dissociation from the heme and subsequent binding of oxygen. This tunnel is in principle capable of delivering the second reactant (NO) to the oxygenated protein. Mutating the FB10 to Leu has consequences for the shape and the connectivity between cavities.

Ligand migration through several temporary docking sites was experimentally detected from the analysis of the geminate rebinding phase following photodissociation of the CO complex of AHb1 [15,21–23]. To detect the migration of the ligand with higher sensitivity in the geminate phase we embedded proteins in silica gels, in the presence of viscogenic agents such as glycerol [22,24–34]. Under these experimental conditions, the geminate phase is normally enhanced by reducing the escape probability of the photodissociated ligand. Gel encapsulation and increased viscosity both favor otherwise thermodynamically unstable states such as those associated with the ligand inside the protein matrix [22,24–28].

We decided to take the same approach for studying rHb1, and gain some insight into the reaction pathways of CO after photolysis of the ferrous COrHb1 complex. This will help us compare and understand the diversity or similarity of ligand migration in nsHbs in general. Temperature dependent (at near physiological temperatures) laser flash photolysis experiments on wt rHb1 in solutions and in gels were thus performed and the effect of mutations at FB10 and HE7 positions were evaluated, in view of the relevant role of these residues [16]. Although O_2 and NO are the physiological ligands in the assumed mechanism of rHb1, CO was chosen as a model ligand since it is easily photodissociated in high yield and side oxidation reactions are negligible.

2. Materials and methods

2.1. Expression and purification of recombinant proteins

The gene for wild type protein (rHb1) in pET29a expression vector (Novagen) was provided as a kind gift by Dr. Mark Hargrove of Iowa State University, Ames, USA. FB10L, HE7L, and HE7A mutants were generated from the gene encoding the wild type protein (rHb1) by using QuickChange Site-Directed Mutagenesis Kit from Stratagene. The mutations were confirmed by gene sequencing. Wild type and the mutant genes were heterologously expressed in BL21 Star (λDE3) *E. coli* cells as described previously [16]. Expression of both wild type and mutant proteins were performed in terrific broth media without induction by isopropyl-1-thio-β-D-galactopyranoside. Following inoculation, cells were grown in flasks to an optical density of 0.8 at 37 °C with constant shaking. Subsequently, cells were grown for 16 h at 25 °C and then harvested by centrifugation. Following cell lysis and sonication, the resulting supernatant was bright red in color due to soluble heme bound protein. Purification of wild type protein was achieved by a combination of ammonium sulfate fractionation, Phenyl Sepharose hydrophobic exchange, DEAE Sephadex anion-exchange, and S-200 Sephacryl size-exclusion chromatography as described elsewhere [16]. Mutant proteins were purified in the same way as wild type proteins. A yield of 15–30 mg pure protein was obtained from 5 l of media. The purified protein was reduced and oxidized with an excess of sodium dithionite and potassium ferricyanide respectively, followed by desalting on a G-25 Sephadex column in 20 mM potassium phosphate (pH7.0). The resulting ferric hemoglobin was found to have a Soret/A_{280} absorbance ratio > 3.5 and stored at −80 °C at more than 1 mM concentration in aliquots for further use.

2.2. Sample handling and gel preparation

The encapsulation of rHb1 in silica gels was carried out following a previously described protocol [35]. A solution containing tetramethyl orthosilicate, water and hydrochloric acid was sonicated for 20 min at 4 °C. An equal volume of a deoxygenated solution containing 10 mM phosphate, pH 6.0, was then added to the sol, which was further deoxygenated for 40 min at 4 °C under a flux of nitrogen. Finally, a 200 μM solution of rHb1 (either the wt or one of the above mentioned mutants) in a 50 mM phosphate buffer, pH 7.2, equilibrated with CO at 1 atm, was anaerobically added to the sol. The resulting mixture was layered on quartz plates under anaerobic conditions. Gelation occurred in approximately 20 min. The silica wet gels were anaerobically stored in a buffer containing 100 mM phosphate, 1 mM EDTA, 5 mM sodium dithionite, pH 7.0. Before experiments, the gels were soaked in a solution previously equilibrated with CO. For experiments in high viscosity conditions gels were transferred to 100% glycerol and equilibrated for at least 3 days at 4 °C.

2.3. Kinetic studies

Flash photolysis was carried out with the circularly polarized second harmonic (532 nm) of a Q-switched Nd:YAG laser, and a CW Xe arc lamp as a probe source. The transient absorbance traces were measured at 436 nm through a 0.25-m spectrograph with a 5 stage photomultiplier. The experimental setup was described elsewhere [15,22]. The cuvette had an optical pathlength of 2 mm. The repetition rate was about 0.3 Hz to allow for full sample recovery between laser flashes. A Maximum Entropy Method (MEM) [36,37] was used to retrieve model-independent lifetime distributions, as described previously [22,38]. We have followed the minimal model previously proposed for CO rebinding to AHb1 solutions and gels [15,21,22] and outlined in Scheme 1 to describe the rebinding kinetics. The differential equations associated

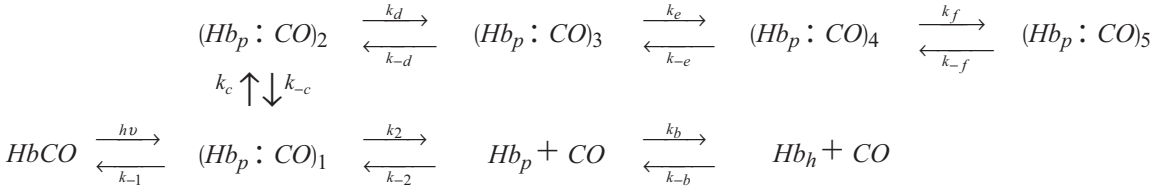

Scheme 1. Minimal reaction scheme for the observed kinetics with sequential migration between internal hydrophobic cavities. After photodissociation of the CO complex of rHb1 (*HbCO*), the photodissociated ligand can migrate to a primary docking site (Hb_p:$CO)_1$, from which it can sequentially access secondary sites (Hb_p:$CO)_2$, (Hb_p:$CO)_3$, (Hb_p:$CO)_4$, (Hb_p:$CO)_5$ or exit to the solvent (Hb_p). The deoxy 5c-HS species (Hb_p) is in equilibrium with the deoxy 6c-LS species (Hb_h).

with Scheme 1 were solved numerically and the rate constants appearing in the equilibrium were optimized to obtain a best fit to the experimental data. Numerical solutions to the set of coupled differential equations corresponding to Scheme 1were determined by using the function ODE15s within Matlab 7.0 (The MathWorks, Inc.). Fitting of the numerical solution to experimental data (and optimization of microscopic rate constants) was obtained with a Matlab version of the optimization package Minuit (CERN).

2.4. Computational modeling

Though crystal structures of wild type rHb1 and FB10L are available in Protein Data Bank, ligand bound structures of these proteins are still lacking. The structures of liganded wild type and mutated rice hemoglobin were thus modeled on the crystal structures of the homologous ligand bound barley hemoglobin (PDB codes 2OIF), [39] which shows 82% sequence identity and 91% similarity to rHb1. The models were built using the homology modeling program MODELLER (http://salilab.org/modeller/), and the side chain orientations further scanned with Sybyl version 8.0 tools (www.tripos.com). The hydrogens were added using the Biopolymer and Build/Edit menu tools and energy-minimized with the Powell algorithm and a gradient of 0.5 kcal $(\text{mol Å})^{-1}$ for 1500 cycles, to remove potentially bad contacts. The analysis of cavity location and accessibility was performed building Connolly surfaces of the whole proteins and of the internal clefts with Sybyl MOLCAD tools, using a sphere probe of 1.4 Å radius [29]. The probe, rolling over the protein accessible areas, builds convex and concave surfaces, according to the presence of atoms well-exposed to the solvent or organized to form clefts and cavities. The cavity depth was calculated by building, over the first molecular surface, a second surface with a 6.0 Å radius probe, so that it is unable to explore smaller cavities. The distance between these two generated surface maps is a direct measure of the cavity depth [40]. Cavities were also directly analyzed with the program PASS freely available on the web (http://www.ccl.net/cca/software/UNIX/pass/overview.shtml) [41]. In order to include the presence of all the hydrogen atoms, the *−hydrogen* option was adopted, thus using a default 1.5 Å radius probe, to investigate the accessibility of the internal tunnels. The area and the volume of the identified cavities were then estimated with the software Grasp (http://trantor.bioc.columbia.edu/grasp/) [42].

The hydrophobic character of the internal cavities was analyzed using the molecular modeling software GRID version 22a (www.moldiscovery.com), [43] using the Xenon atom as an inquiring probe. Energetically and sterically favorable regions are identified by red colored contours.

3. Results

3.1. CO rebinding kinetics to rHb1 in solutions

When CO-wt rHb1 is photodissociated with a nanosecond laser pulse, ligand rebinding occurs with a biphasic time course, with a minor (≈10%) unimolecular nanosecond kinetics, followed by a heterogeneous second order rebinding, accounting for the remainder of the progress curve (Fig. 1A). Rebinding of CO from the solvent encompasses a second order phase in the long microseconds, due to

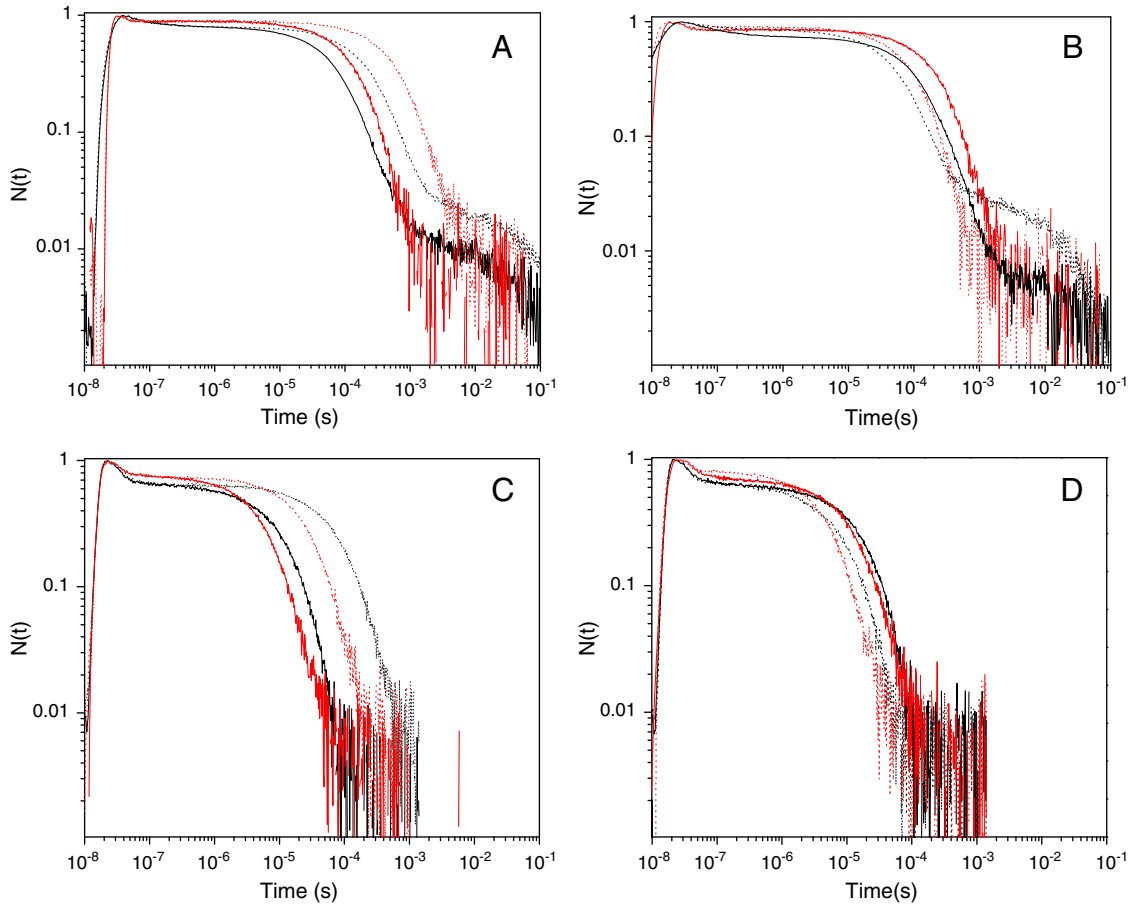

Fig. 1. A: Comparison between CO rebinding kinetics to wt rHb1 (red) and FB10L rHb1 (black), at 20 °C for solutions equilibrated with 1 atm CO (solid) and 0.1 atm CO (dotted). B: Comparison between CO rebinding kinetics to wt rHb1 (red) and FB10L rHb1 (black) at 10 °C (solid) and 30 °C (dotted) at 1 atm CO. C: Comparison between CO rebinding kinetics to HE7L rHb1 (red) and HE7A rHb1 (black) at 1 (solid) and 0.1 (dotted) atm CO, 20 °C. D: Comparison between CO rebinding kinetics to HE7L rHb1 (red) and HE7A rHb1 (black) at 10 °C (solid) and 30 °C (dotted). Solutions were equilibrated with 1 atm CO.

rebinding to pentacoordinated heme, followed by a slower, barely detectable recombination step, due to rebinding to the minor fraction of the heme which has been hexacoordinated by the distal His before CO rebinding occurs.

Panels C and D in Fig. 1 show that replacement of the distal His with a Leu or Ala residue increases the extent of geminate recombination (≈22%), leads to a much faster second order rebinding, and, as expected, prevents the hexacoordination. The FB10L substitution induces remarkable changes in the geminate recombination, whose amplitude (≈18%) is intermediate between those observed for wt rHb1 and HE7L rHb1, and with a more extended character. Second order rebinding occurs with an apparent rate which is intermediate between those observed for wt rHb1 and HE7L and HE7A mutants. A major difference is induced by FB10L in the probability for hexacoordination by the distal His, which now occurs in a higher yield (Fig. 1A and B).

All kinetic phases are thermally activated to some extent, as shown in Fig. 1B and D. The wt protein exhibits the smallest change in the amplitude of the geminate phase when temperature is changed between 10 and 40 °C. Temperature sensitivity is more pronounced for the HE7L and the FB10L mutants. This finding suggests that mutations at E7 and B10 introduce higher barriers along the pathways for ligand exit to the solvent. However, the HE7A mutation appears to obliterate any temperature sensitivity in the geminate phase, suggesting that enthalpic barriers for the innermost rebinding step and exit to the solvent are negligible.

A minimal reaction scheme (Scheme 1) which allows a satisfactory description of the CO rebinding kinetics to wt rHb1 and its FB10L, HE7L, and HE7A mutants comprises the following features. Except for the case of the E7 mutants, CO photodissociation triggers binding of the distal His to the heme Fe, which occurs on the millisecond time scale. Dissociation of the HE7-Fe bond is a slower process, with the rate in the 10 s^{-1} range [16]. An appreciable geminate phase is observed for the wt protein and in the case of the FB10L and the E7 mutants this kinetic phase appears to be extended in time, showing that some reaction intermediates must be considered when describing it. Maximum entropy analysis confirms that geminate phase is indeed heterogeneous (data not shown) and requires the use of more than one kinetic step. These reaction intermediates may be interpreted as arising from rebinding of CO from temporary docking sites located inside the protein matrix. Up to 4 reaction intermediates are necessary to fit some of the rebinding kinetics reported in the following.

Fig. 2 reports the best fits obtained for the CO rebinding kinetics to wt rHb1, FB10L rHb1, HE7L rHb1 and HE7A rHb1 under selected conditions, using the kinetic Scheme 1. Microscopic rate constants along with activation entropies and enthalpies are summarized in Table 1. Table 2 reports the activation free energies estimated at 20 °C.

A peculiar difference between the geminate phase for the wt protein and the mutants is the presence of ligand migration fingerprints in the rebinding kinetics of the mutated proteins. Thus, in order to model this phase properly for rHb1 mutants, we had to introduce a minimum of two reaction intermediates with the CO docked into temporary sites (Fig. 2B, C, and D). The docking sites are populated quickly upon photodissociation, and can host the ligand for relatively long times, extending to the long microseconds.

The change in geminate phase in rHb1 mutants in comparison to the wt protein appears to originate both from effects on the exit (k_2) and the rebinding (k_{-1}) rates. The rate k_{-1} of the innermost binding step suffers a ~2-fold decrease in the FB10L mutant, while it undergoes a ~2-fold increase for HE7L rHb1 and for HE7A rHb1. The innermost step invariably has a small enthalpic barrier, which makes its rate scantly sensitive to temperature. The corresponding free energy barrier is on the order of 8 kcal/mol for the wt and the FB10L mutant. This barrier drops by half a kcal for the mutants at the E7 position. The small enthalpic barrier for k_{-1} in the investigated temperature range resembles previous findings for myoglobin, human HbA, and Ngb.

Exit rate to the solvent (k_2) is lower for FB10L (~3.7-fold) and HE7A/L (~2-fold) mutants, leading to a larger geminate recombination. The increased activation enthalpy accounts for the observed higher temperature sensitivity. At variance, in the case of the HE7A mutant the enthalpic barrier is essentially negligible, leading to small changes with temperature in geminate recombination amplitude and rate (Fig. 1D). The free energy barrier for k_2 shows very little variations across investigated proteins, with wt rHb1 being characterized by the lowest value, and the FB10L mutant having the highest.

Mutations at the E7 position lead to a remarkable increase in the rate k_{-2} (about 10-fold for HE7L), with activation enthalpies heavily reduced, and a ca. 1 kcal/mol reduction in the free energy barrier. A more modest effect is observed for FB10L.

The binding rate (k_b) for the distal His is increased while the dissociation rate (k_{-b}) is decreased for FB10L mutant relative to wt rHb1. The equilibrium constant between the bis-histidyl hexa- and the pentacoordinated species ($K_H \approx 10.9$) is higher than for wt rHb1 ($K_H \approx 1.2$), in agreement with literature data [16]. As a consequence, the reduced deoxy wt protein shows an equilibrium between the 5c and 6c species, while the FB10L mutant is essentially fully hexacoordinated.

By contrast the value of K_H in AHb1 is lower for FB10L ($K_H \approx 0.5$) than for wt AHb1 ($K_H \approx 1.6$), [20] an indication that FB10 has effects of an opposite sign on hexacoordination in the two nsHbs.

It is useful to estimate the bimolecular binding rate constant ($k_{ON} = k_{-2}\, k_{-1}/(k_{-1} + k_2)$) which is 8.3×10^6 M^{-1} s^{-1} for wt rHb1 at 20 °C and becomes 20.7×10^6 M^{-1} s^{-1} for FB10L, 24.5×10^7 M^{-1} s^{-1} for HE7L, and 15.4×10^7 M^{-1} s^{-1} for HE7A. Prior determinations of k_{ON} for wt rHb1 are in full agreement with our estimate ($k_{ON} = 7 \times 10^6$ M^{-1} s^{-1} [16]). Literature values for FB10L and HE7L mutants ($k_{ON} = 9 \times 10^6$ M^{-1} s^{-1} and $k_{ON} = 40 \times 10^7$ M^{-1} s^{-1}, respectively) appear less consistent with our determination, but fall within a factor of 2.

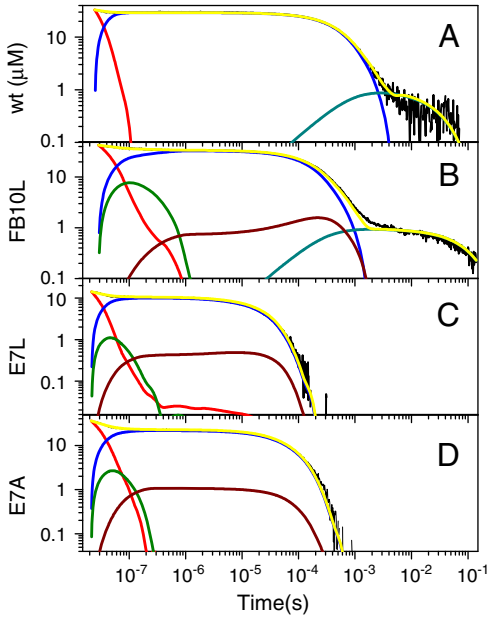

Fig. 2. Analysis of the CO binding kinetics to wt rHb1 (A), FB10L rHb1 (B), HE7L rHb1 (C), and HE7A rHb1 (D) in solution equilibrated at 0.1 atm CO and at T = 20 °C. Vertical axis reports the concentration of deoxy species in μM. The fit (yellow lines) are superimposed on the experimental data (black straight lines). The time course of relevant species in Scheme 1 is also shown: $(Hb_p{:}CO)_1$, red; $(Hb_p{:}CO)_2$, green; $(Hb_p{:}CO)_3$, brown; Hb_p, blue; Hb_h, cyan.

Table 1
CO rebinding to rHb1 in solutions. Microscopic rate constants at T = 20 °C and activation entropies and enthalpies determined from Eyring plots in the temperature range 10–40 °C.

	wt			FB10L			HE7L			HE7A		
		$\Delta H^{\ddagger}$ (kcal/mol)	$\Delta S^{\ddagger}$ (cal/kmol)		$\Delta H^{\ddagger}$ (kcal/mol)	$\Delta S^{\ddagger}$ (cal/kmol)		$\Delta H^{\ddagger}$ (kcal/mol)	$\Delta S^{\ddagger}$ (cal/kmol)		$\Delta H^{\ddagger}$ (Kcal/mol)	$\Delta S^{\ddagger}$ (cal/kmol)
k_{-1} (10^6 s^{-1})	9.2	0.17 ± 0.01	−26.03 ± 0.04	5.09	0.62 ± 0.05	−25.7 ± 0.2	17.41	1.1 ± 0.1	−21.6 ± 0.4	19.2	0.4 ± 0.2	−23.7 ± 0.6
k_2 (10^6 s^{-1})	73.3	4.3 ± 0.3	−7.97 ± 0.95	19.5	6.1 ± 0.3	−4.2 ± 0.9	48.5	6.0 ± 0.2	−2.8 ± 0.7	32	0.14 ± 0.03	−19.1 ± 0.1
k_{-2} (10^6 M^{-1} s^{-1})	74.8	12.4 ± 0.4	20.0 ± 1.4	100	10.9 ± 0.5	15 ± 2	928.36	5.1 ± 0.4	−0.1 ± 1.4	410	8.3 ± 0.5	9.5 ± 1.7
k_b (s^{-1})	50	15.5 ± 0.3	2.1 ± 1.1	120	18.3 ± 1.2	14 ± 4		–	–		–	–
k_{-b} (s^{-1})	40	14.0 ± 0.3	−3.4 ± 0.9	11	12.5 ± 1.2	−11 ± 4		–	–		–	–
k_c (10^6 s^{-1})		–	–	8	7.5 ± 1.3	−1.2 ± 4.4	10	3.0 ± 0.1	−16.2 ± 0.3	7.5	1.60 ± 0.03	−21.4 ± 60.12
k_{-c} (10^6 s^{-1})		–	–	4.6	5.2 ± 0.3	−10 ± 1	20	7.2 ± 0.2	−0.7 ± 0.7	16	0.61 ± 0.03	−23.2 ± 0.1
k_d (10^6 s^{-1})		–	–	0.26	7.7 ± 0.7	−7.6 ± 2.5	5	5.4 ± 0.3	−9.6 ± 0.9	4.3	4.1 ± 0.3	−14 ± 1
k_{-d} (10^6 s^{-1})		–	–	0.0029	11.5 ± 1.2	−3.2 ± 4.1	0.08	3.8 ± 0.1	−23.0 ± 0.3	0.038	5.6 ± 0.5	−18 ± 2

3.2. CO rebinding kinetics to rHb1 in gels

In order to better expose the ligand migration processes, we have encapsulated the CO complexes of rHb1 and its mutants into silica gels and measured the resulting rebinding kinetics after laser photolysis. Fig. 3 compares the kinetics observed for rHbs in solutions and in gels. In general, the geminate recombination is greatly enhanced, the largest effect being observed for the FB10L mutant, for which geminate phase is increased from about 20% in solution to nearly 60% in the gel. More moderate enhancement is observed for wt rHb1 (from ≈10% to ≈20%), for HE7L rHb1 (from ≈22% to ≈30%), and for HE7A rHb1 (from ≈40% to ≈60%). In addition, the geminate rebinding kinetics appears more heterogeneous, indicating that reaction intermediates contribute to the observed signal. Gel encapsulation results in a strong inhibition of hexacoordination of the heme by the distal His, as can be judged by the kinetic traces in Fig. 3A.

Fitting of the data was achieved using kinetic Scheme 1 as well, and the rebinding signal required indeed the use of multiple reaction intermediates in the geminate phase (Fig. 4). Microscopic rates and activation entropies and enthalpies are reported in Table 3. Table 4 reports the activation free energies estimated at 20 °C. The effect on the innermost step (k_{-1}) is to increase the rate for the wt rHb1 and, to a larger extent, the FB10L mutant. More modest increments are observed for the HE7 mutants. Small effects are observed on k_2 for wt rHb1 and FB10L rHb1, while a stronger reduction (about 2-fold) in the exit rate is observed for both HE7 mutants. The FB10L mutant shows the largest effect on the rebinding rate k_{-2}, which undergoes a 2-fold decrease.

The gel exerts a relevant effect on the distal His dissociation rates for both the wt protein and the FB10L mutant resulting in lower equilibrium binding constants K_H (for wt rHb1 it becomes 0.8 and for FB10L it drops to about 5).

Analysis of the rebinding kinetics to wt rHb1 gels indicates the presence of (at least) two reaction intermediates where CO is temporarily docked into internal locations of the protein. The presence of internal migration pathways is common to all investigated mutants, but each of them has characteristic features showing that the structures of the internal cavities are affected by the selected mutations. Thus, the distal pair of E7 His and B10 Phe, selected naturally over evolution, is essential to the physiological function of the proteins since only this combination will produce the requisite kinetic characteristics *in vivo*.

When wt rHb1 gels are soaked in glycerol, the geminate rebinding becomes overwhelmingly large and hexacoordination appears to vanish (Fig. 5). A very minor second order phase is left under these conditions. This increase in geminate recombination is apparent also

Table 2
CO rebinding to rHb1 in solutions. Activation free energies at 20 °C from the activation entropies and energies reported in Table 1.

	wt	FB10L	HE7L	HE7A
	$\Delta G^{\ddagger}$ (kcal/mol)	$\Delta G^{\ddagger}$ (kcal/mol)	$\Delta G^{\ddagger}$ (kcal/mol)	$\Delta G^{\ddagger}$ (kcal/mol)
k_{-1}	7.8	8.0	7.3	7.3
k_2	6.6	7.2	6.7	7.0
k_{-2}	6.5	6.3	5.0	5.6
k_b	14.7	14.2	–	–
k_{-b}	14.9	15.5	–	–
k_c	–	7.6	7.6	7.9
k_{-c}	–	8.0	7.3	7.4
k_d	–	9.8	8.1	8.2
k_{-d}	–	12.3	10.5	10.9

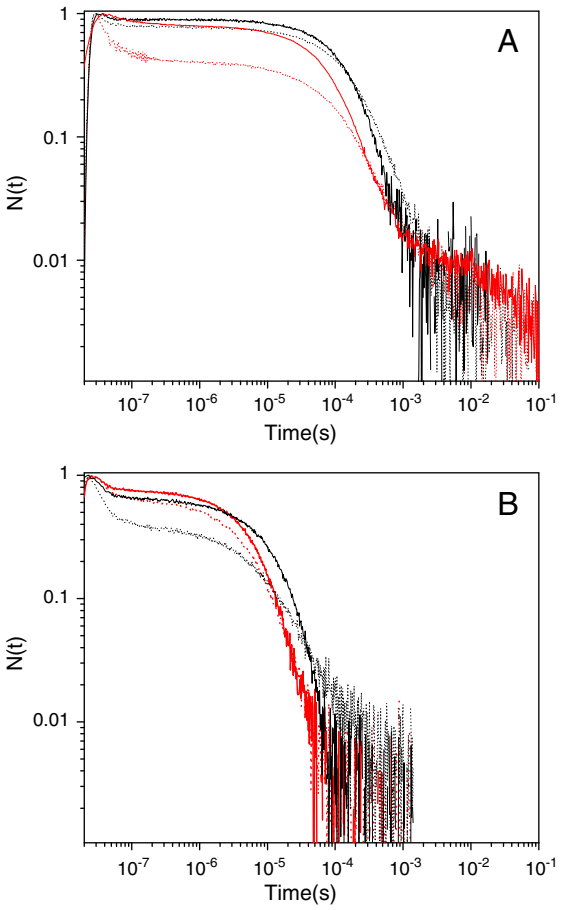

Fig. 3. A. Comparison between CO rebinding kinetics after laser flash photolysis of CO-wt rHb1 (black) and FB10L rHb1 (red), in solution (solid) and embedded in the gel (dotted). T = 20 °C, 1 atm CO. B. Comparison between CO rebinding kinetics after laser flash photolysis of CO HE7L rHb1 (red) and HE7A rHb1 (black), in solution (solid) and embedded in the gel (dotted). T = 20 °C, 1 atm CO.

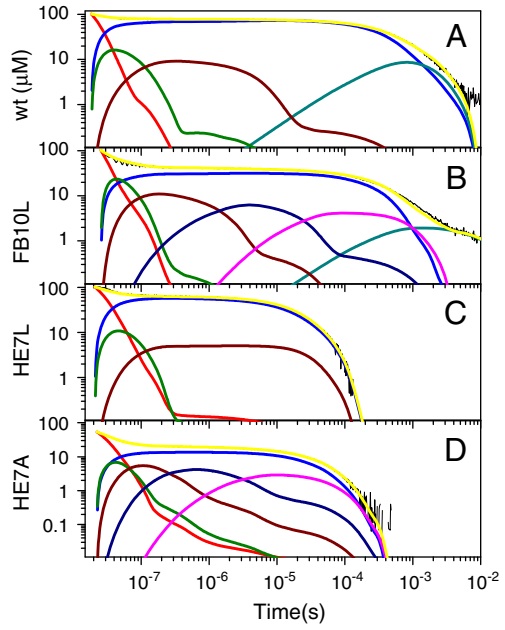

Fig. 4. Analysis of the CO binding kinetics to wt rHb1 (A), FB10L (B), HE7L (C) and HE7A (D) gels at CO = 0.1 atm and 20 °C. The fit (yellow line) is superimposed on the experimental data (black open circle). The time course of relevant species in Scheme 1 is also shown: (Hb_p:CO), red; $(Hb_p:CO)_1$, green; $(Hb_p:CO)_2$, brown; $(Hb_p:CO)_3$, navy; $(Hb_p:CO)_4$, magenta; Hb_p, blue; Hb_h, cyan.

for the FB10L mutant, for which, however, the progress curve is very distributed in time and is completely lacking a second order phase as the signals display no CO concentration dependence (data not shown). This indirectly shows that His hexacoordination is hindered under these conditions.

Analysis of the rebinding curves with kinetic Scheme 1 is reported in Fig. 6. Only one docking site is reached by the photodissociated ligand for the wt protein. The constraints of the gel and the high bulk viscosity of glycerol both dramatically increase the rebinding rate k_{-1} (10-fold) and decrease the exit rate (k_2), the latter rate experiencing a higher enthalpic barrier (Table 5). Exchange of the ligand with the solvent is highly hindered under these conditions also when we consider the rebinding rate (k_{-2}). This shows that the protein needs to preserve a higher degree of flexibility to allow for an efficient exchange of ligands.

Just like wt rHb1, mutant FB10L also shows enhancement in k_{-1} when gels are soaked in glycerol. At variance, no exit of the photodissociated ligand is observed, rather only sampling of 4 internal docking sites characterized by distinct rebinding rates.

3.3. Computational analysis of internal cavities

In order to identify possible migration pathways in the structure of rHb1, we have performed a computational analysis of the internal cavities, their connectivity, and their communication with the solvent.

The crystallographic hexacoordinated form of wt rHb1 (PDB code 1d8u) [44] displays a very small and isolated distal cavity (Fig. 7) lined by residues Phe40, Phe41, Ile44, Phe45, Phe55, Val78 and Tyr151. The cavity appears to be connected to the solvent, thanks to the position of Phe45 which, differently from what occurs in the liganded model (see Fig. 8A), opens up and makes the distal pocket directly solvent accessible. This can be appreciated in the right panel to Fig. 7, in which the long tunnel extends from the distal cavity to the left, to reaches the solvent.

The relevant structure in nanosecond laser flash photolysis experiments is the liganded species, since hexacoordination by the distal His occurs to a low extent during rebinding and affects only the long time scale of the kinetics. The photodissociated CO thus migrates through a pentacoordinated, unrelaxed (or partly relaxed) structure. Unfortunately only the crystal structure of the deoxy, bis-histidyl species is available for both wtrHb1 and FB10L rHb1; thus we have modeled the structure of the liganded species by using the available structure of the highly related ligand bound barley nsHb [39] as a template. Analysis of the internal cavities in the wt model of the liganded rHb1 (Fig. 8A) identifies the presence of two large channels. The first is located in the distal cavity and delimited by Phe40, Phe41, Phe45, Phe55, Phe57, His74 (corresponding to HE7), Tyr145 and Leu126. Leu126 also regulates the connection with a secondary docking site lined by Trp26 and Trp147, which is directly connected with the external solvent. The direct communication of the protein matrix with the solvent may explain the relatively poor geminate rebinding reported for wt rHb1, since this second channel could be exploited by small ligands as a way out to leave the protein after photolysis, quickly passing through the internal hydrophobic cavities. In the FB10L mutant, substitution of phenylalanine B10 with a less bulky residue clearly enlarges the accessible volume of the distal cleft (Fig. 8B), while the second site appears extremely reduced and not easily reachable. No direct connection with the solvent is identified, thus supporting the higher geminate rebinding, and also the slower bimolecular rebinding, with respect to the wt case. Generally, a 30% decrease in the volume of the cavities has been estimated (Table 6). A hindered exchange of the ligand between the solvent and the distal heme pocket is in keeping with the lack of a second order phase for gel soaked in glycerol, showing that the ligand cannot escape to the solvent when the protein experiences high viscosity conditions.

In the HE7L mutant the secondary docking site is again present, even if the communication with the distal pocket appears to be extremely hard and restricted by Tyr145 rather than by Leu126

Table 3
CO rebinding to rHb1 gels. Microscopic rate constants at T = 20 °C and activation entropies and enthalpies determined from Eyring plots in the temperature range 10–40 °C.

	wt			FB10L			HE7L			HE7A		
		$\Delta H^{\ddagger}$ (kcal/mol)	$\Delta S^{\ddagger}$ (kcal/kmol)		$\Delta H^{\ddagger}$ (kcal/mol)	$\Delta S^{\ddagger}$ (cal/kmol)		$\Delta H^{\ddagger}$ (kcal/mol)	$\Delta S^{\ddagger}$ (cal/kmol)		$\Delta H^{\ddagger}$ (kcal/mol)	$\Delta S^{\ddagger}$ (cal/kmol)
k_{-1} (10^6 s^{-1})	19.48	≈0	−25.0	39.12	1.8 ± 0.1	−17.5 ± 0.4	21.4	0.98 ± 0.01	−21.58 ± 0.04	34.8	0.37 ± 0.01	−22.45 ± 0.01
k_2 (10^6 s^{-1})	65.0	4.3 ± 0.3	−8.0 ± 0.9	19.99	6.4 ± 0.4	−3.1 ± 0.1	32	4.7 ± 0.4	−8.2 ± 0.3	14	2.7 ± 0.1	−16.5 ± 0.5
k_{-2} (10^6 M^{-1} s^{-1})	60.28	11.1 ± 0.7	15 ± 2	19.24	11.8 ± 0.9	14.9 ± 3.1	935.5	4.9 ± 0.4	0 ± 1	311.7	5.5 ± 0.4	−1 ± 1
k_b (s^{-1})	45.1	3.0 ± 0.1	−40.5 ± 0.5	150	10.5 ± 0.6	−13 ± 2		–	–		–	–
k_{-b} (s^{-1})	54.9	2.4 ± 0.1	−42.4 ± 0.3	30	4.7 ± 0.3	−36 ± 1		–	–		–	–
k_c (10^6 s^{-1})	9	3.0 ± 0.1	−16.4 ± 0.4	38.99	2.2 ± 0.2	−16 ± 1	12	4.7 ± 0.3	−10 ± 1	18.8	4.5 ± 0.3	−10 ± 1
k_{-c} (10^6 s^{-1})	3	8.6 ± 0.7	0 ± 2	29.0	2.5 ± 0.2	−15.7 ± 0.7	18	4.7 ± 0.3	−9 ± 1	26	3.1 ± 0.1	−13.8 ± 0.5
k_d (10^6 s^{-1})	2.5	5.7 ± 0.4	−10 ± 2	7.46	4.3 ± 0.7	−12 ± 2	5.3	5.4 ± 0.4	−9 ± 1	21	4.0 ± 0.2	−11.4 ± 0.7
k_{-d} (10^6 s^{-1})	0.0045	7.1 ± 0.6	−18 ± 2	0.480	1.2 ± 0.1	−28.2 ± 0.2	0.080	3.4 ± 0.2	−24.2 ± 0.6	3	2.7 ± 0.1	−19.7 ± 0.3
k_e (10^6 s^{-1})		–	–	0.47	1.3 ± 0.1	−28.0 ± 0.4		–	–	3.6	2.1 ± 0.1	−21.1 ± 0.2
k_{-e} (10^6 s^{-1})		–	–	0.039	1.6 ± 0.2	−32.0 ± 0.6		–	–	0.56	1.19 ± 0.02	−28.01 ± 0.07
k_f (10^6 s^{-1})		–	–	0.030	2.2 ± 0.2	−30.3 ± 0.7		–	–	0.26	3.1 ± 0.1	−22.8 ± 0.5
k_{-f} (10^6 s^{-1})		–	–	0.0033	2.7 ± 0.3	−33 ± 1		–	–	0.06	10.6 ± 0.5	0 ± 2

Table 4
CO rebinding to rHb1 gels. Activation free energies at 20 °C from the activation entropies and energies reported in Table 1.

	wt	FB10L	HE7L	HE7A
	$\Delta G^{\ddagger}$ (kcal/mol)	$\Delta G^{\ddagger}$ (kcal/mol)	$\Delta G^{\ddagger}$ (kcal/mol)	$\Delta G^{\ddagger}$ (kcal/mol)
k_{-1}	7.3	6.9	7.3	7.0
k_2	6.6	7.3	7.1	7.5
k_{-2}	6.7	7.4	5.1	5.7
k_b	14.8	14.1	–	–
k_{-b}	14.7	15.1	–	–
k_c	7.8	6.9	7.6	7.3
k_{-c}	8.4	7.1	7.4	7.2
k_d	8.5	7.8	8.1	7.3
k_{-d}	12.2	9.5	10.5	8.4
k_e	–	9.5	–	8.2
k_{-e}	–	10.9	–	9.4
k_f	–	11.1	–	9.8
k_{-f}	–	12.4	–	10.6

(Fig. 8C). Nevertheless, even if no direct connection with the exterior is available through the secondary tunnel, a new channel is opened on the side of the heme between the distal pocket and secondary docking site (black arrow in Fig. 8C) and could explain the extremely high rates for exit and for bimolecular rebinding. The volume of the cavities is quite similar to the FB10L mutant. On the contrary, a significant increase in size has been measured for the HE7A mutant (Table 6 and Fig. 8D), which displays an extremely large and complex system of internal clefts and channels. The previous connection with the solvent detected for the HE7L mutant is lost, but the substitution of the leucine with a definitely less bulky alanine directly opens the distal site to the solvent. Comparison of the k_2 and k_{-2} velocities, with the respective values measured for the wt protein, clearly suggests that ligands use different channels to enter and leave the protein matrix. In particular the relatively poor k_2 for HE7A rHb1 indicates that after the photolysis the ligands do not leave the protein through the distal pocket, but they have a more hindered escape route possibly through some other cavities, different from that observed for the HE7L mutant (see Tables 1 and 3). On the contrary, the high k_{-2} value indicates that the direct distal entry channel could be used by ligands to rebind to the heme iron at longer times.

With the exception of the HE7A mutant, the distal cavity does not appear to be easily accessible from the exterior through a path similar to the one which supports ligand exchange in myoglobin according to the so-called His-gate mechanism [45,46]. However, alternative

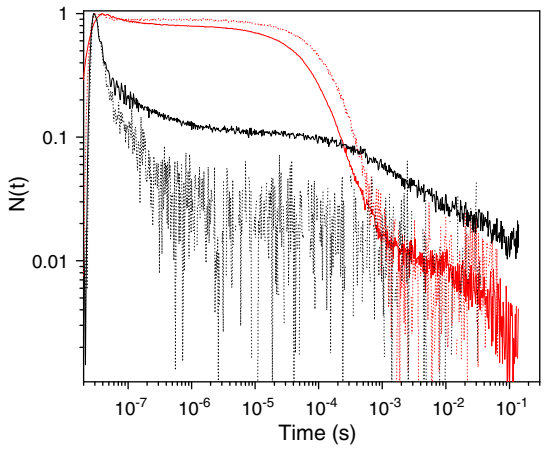

Fig. 5. Comparison between CO rebinding kinetics after laser flash photolysis of wt rHb1 (dotted lines) and FB10L rHb1 (solid lines) in solution (red) and encapsulated in gel and soaked in glycerol (black). T = 20 °C, 1 atm CO.

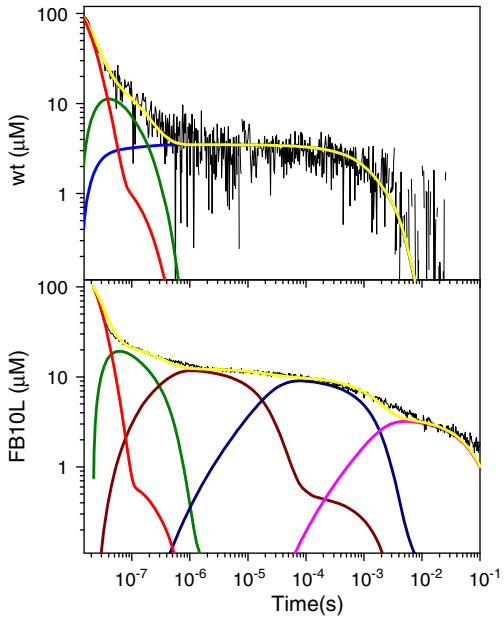

Fig. 6. Analysis of the CO rebinding kinetics to wt rHb1 (top) and FB10L rHB1 (bottom) gels soaked in glycerol at CO = 0.1 atm and T = 20 °C. The fit (yellow line) is superimposed on the experimental data (black open circle). The time course of relevant species in Scheme 1 is also shown: (Hb_p:CO), red; (Hb_p:CO)$_1$, green; (Hb_p:CO)$_2$, brown; (Hb_p:CO)$_3$, navy; (Hb_p:CO)$_4$, magenta; Hb_p, blue.

pathways allow more or less facile exchange of small molecules between the distal pocket and the solvent. Size, shape, and affinity for the ligands of the internal docking pockets are clearly modulated by the mutations at positions B10 or E7.

This effect could be in some way related to the presence of numerous aromatic rings delimiting the cavity and interacting through their systems of delocalized electrons with the CO molecule. The predominant presence of phenylalanine rings in or close to the distal site has been reported in literature for many other globins including barley non-symbiotic hemoglobin, [39] lupin leghemoglobin, [47] neuroglobin, [48,49] and cytoglobin [50] thus suggesting a possible role in regulating the entrance, migration and release of small gaseous molecules, which deserves future investigation.

The role of Phe residues in regulating ligand exchange between binding site, the internal docking sites and the solvent is intimately linked to hexacoordination. As shown in Fig. 7, the peculiar position assumed by Phe45 in the hexacoordinated structure leaves the distal pocket directly accessible from the solvent, while after the ligand entrance (see Fig. 8), the phenyl ring rotates and closes the cavity, hindering the possible exit of the oxygen molecule.

4. Discussion

4.1. Ligand exchange with the solvent

The small geminate rebinding amplitude observed for wt rHb1 suggests that the photodissociated ligand finds a relatively open connection with the exterior, acting as an efficient escape route (Fig. 1A). Temperature has minor effects around physiological values and accordingly points to available exchange routes which facilitate exchange of the ligand with the solvent without the need of substantial thermal motion (Fig. 1B). The relatively high rebinding rate (k_{-1}) and its very low activation enthalpy suggest that the distal His is not imposing a large barrier to rebinding. Thus, there must be a competing escape process which has a comparatively high rate (k_2), so that the resulting amplitude of the geminate phase is small. Among other possibilities, the existence of an escape path, easily accessible

from the distal pocket, would guarantee a high rate for k_2, with an expected mild temperature dependence. The channel identified in Fig. 8A is a likely candidate to play this role.

The effect of mutations at the HE7 position clearly suggests that the distal His regulates the exchange with the solvent. Removal of the distal His increases rebinding rate k_{-1} for both the investigated mutants, thus demonstrating that this residue imposes an appreciable barrier to rebinding. However, the largest effects are on rebinding rates k_{-2}, which are dramatically increased upon mutation and have much lower enthalpic barriers. While a barrier for HE7L is still apparent, although reduced in comparison to the barrier observed for the wt protein, the barrier for HE7A is essentially negligible, suggesting that the small amino acid side chain in this case is not hindering the exchange of the ligand with the distal cavity. Thus, reduction in size of the amino acid side chain at position E7 may favor an exchange through a direct passage (Fig. 8D), which becomes available upon mutation of the distal His. In the case of the HE7L mutant, the exchange channel appears to be distinct and possibly identified with the channel indicated with the arrow in Fig. 8C.

Exit to the solvent (k_2) is hindered by the FB10L mutation, while rebinding (k_{-2}) becomes more likely (Table 1). The system of internal cavities is more structured for FB10L rHb1, but unlike the wt protein, it has no obvious connection to the solvent, and thus is expected to hinder exit of the photodissociated ligand. Rebinding to the heme (k_{-1}) is slower for this mutant, thus compensating for the reduction in escape probability and resulting in a larger geminate amplitude. The return rate k_{-2} drops by 5-fold in gels and becomes negligible when silica gels are soaked in glycerol. This fact demonstrates that the amino acid side chain at B10 position strongly affects the protein dynamics assisting binding from the solvent.

4.2. Ligand migration inside the protein matrix

The geminate rebinding to rHb1 in solutions after photodissociation does not deviate appreciably from a monoexponential relaxation (Fig. 2A and Table 1). This suggests, on one hand, that no internal hydrophobic cavity is accessible to the photodissociated CO molecule under these conditions. In other words, the photodissociated ligand can either reach very easily the solvent through a readily available exit path, or return to the heme for binding. On the other hand, the lack of heterogeneity in the geminate phase also indirectly shows that there is no structural relaxation, affecting protein reactivity on this time scale [51,52]. When the protein is embedded in the pores of the silica gel, the constraints imposed by the matrix are favoring, although in small yield, migration to secondary docking sites, from which CO is rebound at longer times (Fig. 4A and Table 3). As already noted in the previous section, geminate rebinding is enhanced in the gel owing to the 2-fold increase in the rate k_{-1}, but the shape of the progress curve is affected also by ligand migration. The availability of docking sites is further modulated by bulk viscosity, as the population of these reaction intermediates is reduced in comparison to gels soaked in buffered aqueous solutions. Thus, structural flexibility plays a role in allowing access to secondary docking sites.

The FB10 residue has a dramatic effect on geminate rebinding and ligand migration. The B10 appears to impose a substantial barrier to the accessibility of (at least) two reaction intermediates, likely temporary docking sites for the photodissociated CO. When this barrier is removed by substitution with the less bulky Leu, cavities become available (Fig. 3 and Table 1). This effect is enhanced by increasing the bulk viscosity when soaking gels in glycerol. Under these conditions, the internal migration path is not only favored but becomes the only available reaction pathway. Comparison between Fig. 8A and B gives an immediate glimpse of the structural changes leading to reshaping of the internal cavities, which account for the availability of temporary docking sites in the case of FB10L mutant.

The E7 residue is also involved in the regulation of the internal migration pathways. Mutations at E7 either with the relatively bulky Leu or with the much smaller Ala invariably favor migration to internal locations. The effect is similar to the one observed for the FB10L mutation, except that the enthalpic barrier for migration to the first cavity is smaller. The constraints imposed by gel encapsulation play a minor role in modulating migration in these mutants (compare Tables 1 and 3). However, a substantial difference exists between the E7L and the E7A mutations.

The latter introduces a much larger (Table 6) and more structured (Fig. 8C and D) system of cavities, which helps understanding why a lower number of reaction intermediates is identified in the rebinding kinetics to the HE7L mutant.

These effects can be compared to those observed for type 1 nsHb from *A. thaliana* (AHb1). For this protein, a complex system of cavities becomes available after photodissociation of the CO adduct, encapsulated within silica gels, and even more so when soaked in glycerol, leading to several reaction intermediates (Fig. 8) [23]. Molecular dynamics demonstrated that these cavities allow escape of the ligand to the solvent through well defined pathways, and that mutations at the FB10 and HE7 residues strongly affect their three dimensional layout [20]. Both mutations reshape cavities and introduce interruptions in the pathway connecting the distal heme pocket with the solvent, thus enhancing the geminate rebinding probability. The protein matrix in AHb1 hosts a series of interconnected cavities which are capable of trapping ligands and deliver them to the active site (the distal heme pocket). Importantly, a secondary tunnel was shown to become available upon binding of oxygen to the heme, suggesting that this may support the supply of NO to the oxygenated heme, thus sustaining the putative NO dioxygenase reaction of AHb1. A similar structured rebinding was observed for human neuroglobin and cytoglobin gels (Fig. 9), two other hexacoordinated Hbs suggested to display NO dioxygenase activity [18,53].

Table 5
CO rebinding to rHb1 gels soaked in glycerol. Microscopic rate constants at T = 20 °C and activation entropies and enthalpies determined from Eyring plots in the temperature range 10–40 °C. $\Delta G^{\ddagger}$values have been estimated at 20 °C.

	wt				FB10L			
		$\Delta H^{\ddagger}$ (kcal/mol)	$\Delta S^{\ddagger}$ (kal/kmol)	$\Delta G^{\ddagger}$ (kcal/mol)		$\Delta H^{\ddagger}$ (kcal/mol)	$\Delta S^{\ddagger}$ (cal/kmol)	$\Delta G^{\ddagger}$ (kcal/mol)
k_{-1} (10^6 s^{-1})	76.08	≈0	−22.4	7.8	59	1.3 ± 0.2	−18.6 ± 0.6	6.7
k_2 (10^6 s^{-1})	2.69	9.3 ± 0.5	3 ± 1	6.6				
k_{-2} (10^6 M^{-1} s^{-1})	16.69	14 ± 2	24 ± 7	6.5				
k_c (10^6 s^{-1})	13.39	6.5 ± 0.1	−3.8 ± 0.2	14.8	17.25	7.9 ± 0.4	2 ± 1	7.4
k_{-c} (10^6 s^{-1})	11.09	7.7 ± 0.6	0 ± 2	14.9	2.59	2.4 ± 0.3	−21 ± 1	8.5
k_d (10^6 s^{-1})					2.31	5.5 ± 0.4	−11 ± 1	8.6
k_{-d} (10^6 s^{-1})					0.020	6.2 ± 0.7	−18 ± 2	11.3
k_e (10^6 s^{-1})		–	–		0.039	1.0 ± 0.1	−34.1 ± 0.2	11
k_{-e} (10^6 s^{-1})		–	–		0.25	7.4 ± 0.6	−18 ± 2	13
k_f (10^6 s^{-1})		–	–		2.60	10.1 ± 0.6	−13 ± 2	14
k_{-f} (10^6 s^{-1})		–	–		0.2	5.1 ± 0.4	−35 ± 1	15

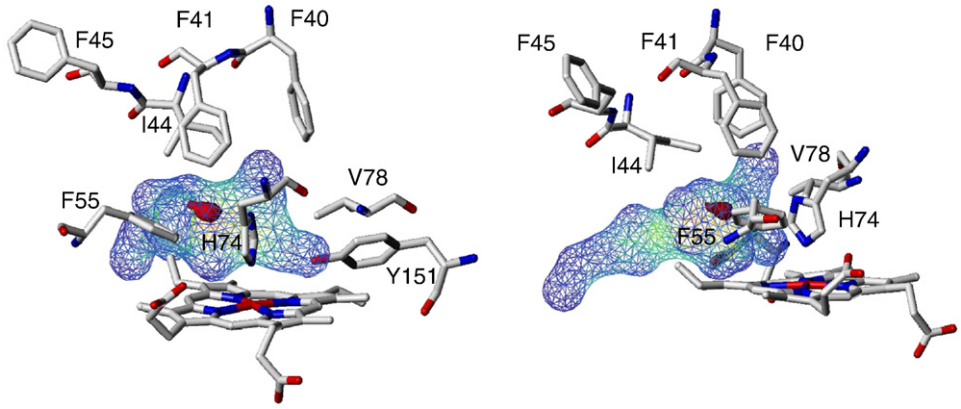

Fig. 7. Cavities identified in the hexacoordinated structures of wt rHb1(PDB code 1d8u) [44]. The volumes of the cavities are displayed by lined Connolly surfaces, while the areas energetically favorable for allocating a hydrophobic xenon probe are identified by GRID red contours. The residues defining the extension and regulating the connection between the internal channels are labeled and shown in capped sticks. For comparison, the left panel presents a view of the distal cavity with the same perspective as in the following Fig. 8. However, the shape of the cavity and its extension to the solvent is better appreciated in the view reported in the right panel.

A common feature to all of these proteins is the low geminate recombination in nanosecond laser flash photolysis experiments, which was invariably taken as a clear indication of the presence of a facilitated reactant exchange route between the reaction site in the distal heme pocket and the solvent. For AHb1 and for rHb1 a clear pathway is apparent from the analysis of the internal cavities which may be functional to support incoming NO molecules, accessing the distal heme pocket of the oxygenated protein.

It should be pointed out that while CO is a widely exploited model ligand to probe heme reactivity and ligand migration pathways, differences are expected in the absolute values of rate constants for NO and O_2 as a consequence of different energetic barriers encountered by these gasses [54]. Differences could possibly be found also in the reaction schemes, as some of the internal docking sites may have a different accessibility for the three diatomic gasses as demonstrated for myoglobin [55].

4.3. Distal His hexacoordination

Laser flash photolysis experiments on the FB10L mutant confirm previous findings which suggested the fundamental role of FB10 in the regulation of heme hexacoordination by the distal His [16]. Experiments reported in this work confirm that hexacoordination is enhanced when the bulky Phe residue is replaced by the linear chain

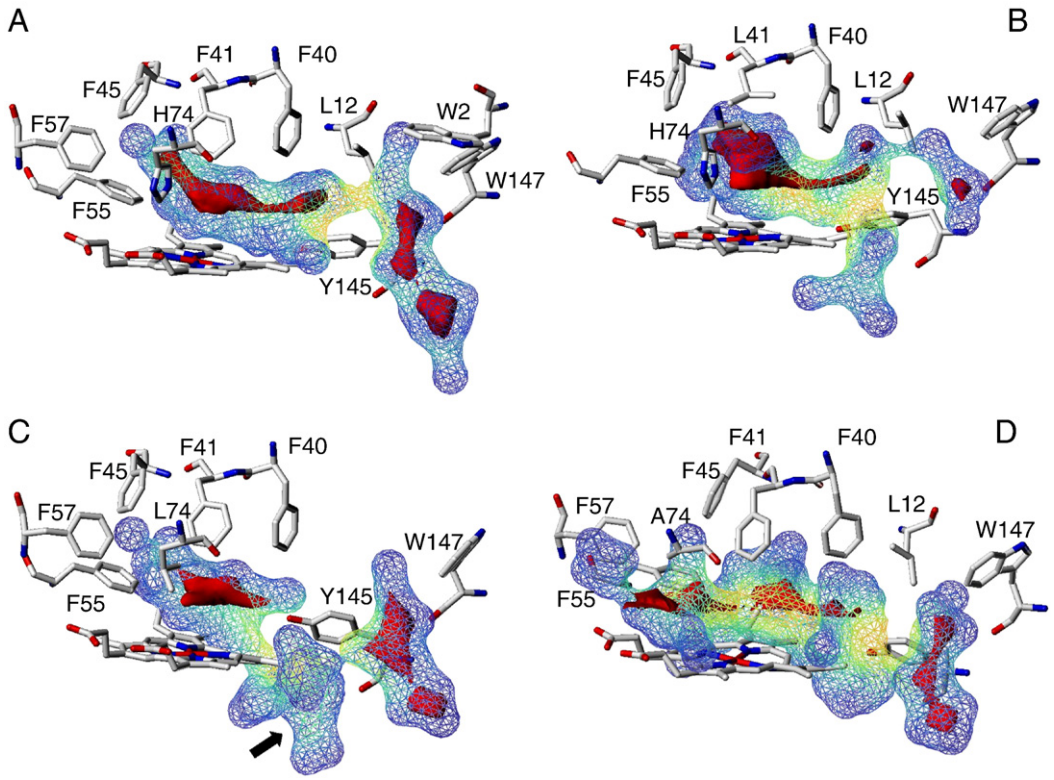

Fig. 8. Cavities identified in the liganded structures of wt (A), FB10L (B), HE7L (C) and HE7A (D) of rHb1 modeled on the crystal structure of barley Hb (PDB code 2OIF [39]). The volumes of the cavities are displayed by lined Connolly surfaces, while the areas energetically favorable for allocating a hydrophobic xenon probe are identified by GRID red contours. The residues defining the extension and regulating the connection between the internal channels are labeled and shown in capped sticks. F41 corresponds to FB10 mutated to L41 in the FB10L mutant (B), while H74 correspond to the distal histidine HE7, mutated to L74 and A74 in the HE7L (C) and HE7A (D) mutants, respectively. The CO occupying the sixth position of coordination has been removed from the analysis to better show the extension of the cavities.

Table 6
Volumes and areas of identified cavities in wt and mutated rHb.

Structure	Volume (Å^3)	Area (Å^2)
wt	418	582
FB10L	283	450
HE7L	291	518
HE7A	444	676

of Leu, which apparently leaves more freedom to the HE7 residue to set on the Fe coordination.

On the other hand, gel encapsulation appears to highly inhibit hexacoordination by the distal His for both the wt and the FB10L mutant. This implies that ligation of the distal His to the heme requires that the protein either goes through an extended transition state, or that the hexacoordinated protein occupies a larger volume than the pentacoordinated one. The size of the gel pore is possibly not capable of accommodating the structural changes brought about by His hexacoordination. The structural changes associated with hexacoordination were clearly identified by Hargrove and coworkers, by comparing the crystal structures of the CN-bound rHb1 and the deoxy hexacoordinated barley Hb [39,44]. The major structural rearrangement accompanying hexacoordination involve shifting of helix E with a piston like movement, and large reshaping of the flexible CD and EF loops which are more extended in comparison to other globins [39]. The gel pore does not allow this reshaping thus partly preventing hexacoordination.

Type 1 nsHbs have moderate His binding constants, such that under physiological conditions these proteins are only partly hexacoordinated, resulting in a mixture of hexa- and pentacoordinated deoxyhemes [8]. At variance, type 2 nsHbs show much higher His binding constants and are fully hexacoordinated both in their ferric or ferrous deoxy states [8].

Residue FB10 was shown to have a profound impact on hexacoordination in rHb1 and mutating this amino acid greatly enhances hexacoordination, thus directly proving a direct interaction between FB10 and HE7, [16] which is likely at the basis of the differences observed with type 2 nsHbs.

FB10 has also a fundamental role in stabilizing bound ligands. It was proposed that once an exogenous ligand (like oxygen) is bound, FB10 forces the HE7 to form a stabilizing hydrogen bond. This conclusion is supported by CO-FTIR spectra of FB10L and HE7L mutant proteins, showing reduced polar interactions in the absence of Phe at position B10, to an extent which is dependent on the specific mutation introduced. While interactions between the bound ligand and the distal His are reduced for all of these mutants, they are not completely removed, as demonstrated by the ν-CO-FTIR spectrum of the HE7L mutant [16]. Similar results were obtained by Resonance Raman spectroscopy of AHb1 and its FB10L and HE7L mutants [15,20].

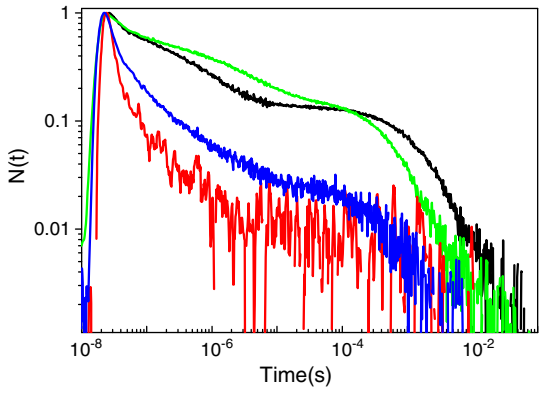

Fig. 9. Comparison between CO rebinding kinetics to rHb1 (red), AHb1 (green), human neuroglobin (blue), and human cyglobin (black) gels soaked in glycerol at T = 10 °C and 1 atm CO.

Interaction of HE7 with the bound ligand through a strong hydrogen bond also supports the stability of the oxyferrous compound against autoxidation [56,57]. The large increase in autoxidation upon B10 mutation is related to removal of these interactions in combination with solvent entry into the distal heme pocket.

4.4. NO scavenging

While to date there is no clear evidence that rHb1 has a role in NO scavenging *in vivo*, NO dioxygease activity was recently studied in detail for rHb1 *in vitro* [11].

Comparison of the efficiency of the NO dioxygease activity *in vitro*, elicited by myoglobin, to that of rHb1 and other hexacoordinated hemoglobins, showed that the latter proteins do not achieve higher performance [11]. Smagghe et al. also demonstrated that the limiting factor in NO scavenging for all Hbs examined in their work is the re-reduction following the NO dioxygenase reaction. Monohydroascorbate reductase was found to increase NO dioxygenase activity of barley nsHb, [14] thus suggesting that identification of a specific reductase may be the key step in the assignment of a NO dioxygenase activity as a physiological function on sound basis.

It is nevertheless worth observing that the stabilization of the oxyferrous compound through interactions between FB10 and HE7 to induce a strong hydrogen bond between the latter and the bound ligand is consistent with NO scavenging since oxyHb is the principal reactant in NO dioxygenation [16]. Conservation of the FB10 in Type 1 nsHbs is also suggestive of such a role, given the evidence which has been accumulated for at least three members of the family, which elicit NO dioxygenase action *in vitro* [12,13].

It has been hypothesized that internal cavities may support NO dioxygenase activity in myoglobin [49,58,59] and neuroglobin [18]. The cavities appear to support the NO dioxygenase activity by providing NO to the oxygenated protein through preferential migration pathways, as demonstrated for truncated Hb N from *Mycobacterium tuberculosis* [60,61]. Ligand migration signatures are invariably found in the CO rebinding kinetics to these proteins [23,28,62]. Our data do not provide clear evidence for complex migration of photodissociated ligands through internal cavities in wt rHb1. However, while two docking sites appear to be available for transient storage of photodissociate ligands in wt rHb1 gels (Fig. 4), the direct channel connecting the distal cavity with the solvent highlighted in the modeled structure points to a facilitated exchange of ligands with the oxygenated protein. Thus, as observed, this may support entry of NO to react with the oxygenated protein.

5. Conclusions

Ligand rebinding kinetics to rHb1 demonstrates that the distal heme cavity in the liganded molecule is directly connected with the solvent, through a tunnel which allows easy access to the reaction site. This tunnel, which is capable to transiently dock photodissociated ligands when viscosity is increased, may be exploited by NO to access the oxygenated distal heme cavity and proceed with the NO dioxygenase reaction. Residues at E7 and B10 positions are important in shaping the internal cavities and define migration pathways. Several Phe residues line the migration pathway and appear to play a role in assisting directional movements of ligands.

Acknowledgements

The authors acknowledge the Italian Ministero dell'Istruzione, dell'Università e della Ricerca (PRIN 2004, 2004052135, PRIN 2008, 2008BFJ34R) and the Department of Biotechnology, Government of India (BT/PR8901/BRB/10/535/2007, BT/01/COE/07/UDSC) for financial assistance. NKB and SU acknowledge receipt of fellowships from the Italian Ministero dell'Istruzione, dell'Università e della Ricerca and

the Council of Scientific and Industrial Research (CSIR), Government of India, respectively.

References

[1] C.A. Appleby, Leghemoglobin and rhizobium respiration, Annu. Rev. Plant Physiol. 35 (1984) 443–478.
[2] D. Bogusz, C.A. Appleby, J. Landsmann, E.S. Dennis, M.J. Trinick, W.J. Peacock, Functioning hemoglobin genes in non-nodulating plants, Nature 331 (1988) 178–180.
[3] R. Arredondo-Peter, M.S. Hargrove, C. Sarath, J.F. Moran, J. Lohrman, J.S. Olson, R.V. Klucas, Rice hemoglobins gene cloning, analysis, and O2-binding kinetics of a recombinant protein synthesized in *Escherichia coli*, Plant Physiol. 115 (1997) 1259–1266.
[4] B. Trevaskis, R.A. Watts, C.R. Andersson, D.J. Llewellyn, M.S. Hargrove, J.S. Olson, E.S. Dennis, W.J. Peacock, Two hemoglobin genes in *Arabidopsis thaliana*: the evolutionary origins of leghemoglobins, Proc. Natl. Acad. Sci. U. S. A. 94 (1997) 12230–12234.
[5] Y.H. Wang, L.V. Kochian, J.J. Doyle, D.F. Garvin, Two tomato non-symbiotic haemoglobin genes are differentially expressed in response to diverse changes in mineral nutrient status, Plant Cell Environ. 26 (2003) 673–680.
[6] P.W. Hunt, R.A. Watts, B. Trevaskis, D.J. Llewelyn, J. Burnell, E.S. Dennis, W.J. Peacock, Expression and evolution of functionally distinct haemoglobin genes in plants, Plant Mol. Biol. 47 (2001) 677–692.
[7] C. Dordas, Nonsymbiotic hemoglobins and stress tolerance in plants, Plant Sci. 176 (2009) 433–440.
[8] B.J. Smagghe, J.A. Hoy, R. Percifield, S. Kundu, M.S. Hargrove, G. Sarath, J.L. Hilbert, R.A. Watts, E.S. Dennis, W.J. Peacock, S. Dewilde, L. Moens, G.C. Blouin, J.S. Olson, C.A. Appleby, Correlations between oxygen affinity and sequence classifications of plant hemoglobins, Biopolymers (2009) 1083–1096.
[9] R. Wang, K. Guegler, S.T. LaBrie, N.M. Crawford, Genomic analysis of a nutrient response in *Arabidopsis* reveals diverse expression patterns and novel metabolic and potential regulatory genes induced by nitrate, Plant Cell 12 (2000) 1491–1509.
[10] X. Nie, R.D. Hill, Mitochondrial respiration and hemoglobin gene expression in barley aleurone tissue, Plant Physiol. 114 (1997) 835–840.
[11] B.J. Smagghe, J.T. Trent III, M.S. Hargrove, NO dioxygenase activity in hemoglobins is ubiquitous in vitro, but limited by reduction in vivo, PLoS ONE 3 (2008) e2039.
[12] M. Perazzolli, P. Dominici, M.C.R. Puertas, E. Zago, J. Zeier, M. Sonoda, C. Lamb, M. Delledonne, Non-symbiotic hemoglobin AHb1 modulates nitric oxyde bioactivity in *Arabidopsis thaliana*, Plant Cell 16 (2004) 2785–2794.
[13] M. Perazzolli, M.C. Romero-Puertas, M. Delledonne, Modulation of nitric oxide bioactivity by plant haemoglobins, J. Exp. Bot. 57 (2006) 479–488.
[14] A.U. Igamberdiev, N.V. Bykova, R.D. Hill, Nitric oxide scavenging by barley hemoglobin is facilitated by a monodehydroascorbate reductase-mediated ascorbate reduction of methemoglobin, Planta 223 (2006) 1033–1040.
[15] S. Bruno, S. Faggiano, F. Spyrakis, A. Mozzarelli, S. Abbruzzetti, E. Grandi, C. Viappiani, A. Feis, S. Mackowiak, G. Smulevich, E. Cacciatori, P. Dominici, The reactivity with CO of AHb1 and AHb2 from *Arabidopsis thaliana* is controlled by the distal His E7 and internal hydrophobic cavities, J. Am. Chem. Soc. 129 (2007) 2880–2889.
[16] B.J. Smagghe, S. Kundu, J.A. Hoy, P. Halder, T.R. Weiland, A. Savage, A. Venugopal, M. Goodman, S. Premer, M.S. Hargrove, Role of phenylalanine B10 in plant nonsymbiotic hemoglobins, Biochemistry 45 (2006) 9735–9745.
[17] F. Spyrakis, S. Faggiano, S. Abbruzzetti, P. Dominici, E. Cacciatori, A. Astegno, E. Droghetti, A. Feis, G. Smulevich, S. Bruno, A. Mozzarelli, P. Cozzini, C. Viappiani, A. Bidon-Chanal, F.J. Luque, Histidine E7 dynamics modulates ligand exchange between distal pocket and solvent in AHb1 from *Arabidopsis thaliana*, J. Phys. Chem. B (in preparation).
[18] M. Brunori, A. Giuffrè, K. Nienhaus, G.U. Nienhaus, F.M. Scandurra, B. Vallone, Neuroglobin, nitric oxide, and oxygen: functional pathways and conformational changes, Proc. Natl. Acad. Sci. U. S. A. 102 (2005) 8483–8488.
[19] B. Vallone, K. Nienhaus, K. Matthes, M. Brunori, G.U. Nienhaus, The structure of murine neuroglobin: novel pathways for ligand migration and binding, Proteins 56 (2004) 85.
[20] S. Faggiano, S. Abbruzzetti, F. Spyrakis, E. Grandi, C. Viappiani, S. Bruno, A. Mozzarelli, P. Cozzini, A. Astegno, P. Dominici, S. Brogioni, A. Feis, G. Smulevich, O. Carrillo, P. Schmidtke, A. Bidon-Chanal, F.J. Luque, Structural plasticity and functional implications of internal cavities in distal mutants of Type 1 non-symbiotic hemoglobin AHb1 from *Arabidopsis thaliana*, J. Phys. Chem. B 113 (2009) 16028–16038.
[21] S. Bruno, S. Faggiano, F. Spyrakis, A. Mozzarelli, E. Cacciatori, P. Dominici, E. Grandi, S. Abbruzzetti, C. Viappiani, Different roles of protein dynamics and ligand migration in non-symbiotic hemoglobins AHb1 and AHb2 from *Arabidopsis thaliana*, Gene 398 (2007) 224–233.
[22] S. Abbruzzetti, S. Bruno, S. Faggiano, E. Grandi, A. Mozzarelli, C. Viappiani, Monitoring haem proteins at work with nanosecond laser flash photolysis, Photochem. Photobiol. Sci. 5 (2006) 1109–1120.
[23] S. Abbruzzetti, E. Grandi, S. Bruno, S. Faggiano, F. Spyrakis, A. Mozzarelli, P. Dominici, C. Viappiani, Ligand migration in non symbiotic hemoglobin AHb1 from *Arabidopsis thaliana*, J. Phys. Chem. B 111 (2007) 12582–12590.
[24] S. Abbruzzetti, C. Viappiani, S. Bruno, A. Mozzarelli, Enhanced geminate ligand rebinding upon photo-dissociation of silica gel-embedded myoglobin-CO, Chem. Phys. Lett. 346 (2001) 430–436.
[25] S. Abbruzzetti, C. Viappiani, S. Bruno, S. Bettati, M. Bonaccio, A. Mozzarelli, Functional characterization of heme proteins encapsulated in wet nanoporous silica gels, J. Nanosci. Nanotech. 1 (2001) 407–415.
[26] S. Sottini, C. Viappiani, L. Ronda, S. Bettati, A. Mozzarelli, CO rebinding kinetics to myoglobin- and R state hemoglobin-doped silica gels in the presence of glycerol, J. Phys. Chem. B 108 (2004) 8475–8484.
[27] S. Sottini, S. Abbruzzetti, C. Viappiani, S. Bettati, L. Ronda, A. Mozzarelli, Evidence for two geminate rebinding states following laser photolysis of R state hemoglobin encapsulated in wet silica gels, J. Phys. Chem. B 109 (2005) 11411–11413.
[28] S. Sottini, S. Abbruzzetti, C. Viappiani, L. Ronda, A. Mozzarelli, Determination of microscopic rate constants for CO binding and migration in myoglobin encapsulated in silica gels, J. Phys. Chem. B 109 (2005) 19523–19528.
[29] S. Sottini, S. Abbruzzetti, F. Spyrakis, S. Bettati, L. Ronda, A. Mozzarelli, C. Viappiani, Geminate rebinding in R state hemoglobin: kinetic and computational evidence for multiple hydrophobic pockets, J. Am. Chem. Soc. 127 (2005) 17427–17432.
[30] I. Khan, C.F. Shannon, D. Dantsker, A.J. Friedman, J. Perez-Gonzales-de-Apodaca, J.M. Friedman, Sol–gel trapping of functional intermediates of hemoglobin: geminate and bimolecular recombination studies, Biochemistry 39 (2000) 16099–16109.
[31] U. Samuni, D. Dantsker, I. Khan, A.J. Friedman, E. Peterson, J.M. Friedman, Spectroscopically and kinetically distinct conformational populations of sol–gel-encapsulated carbonmonoxy myoglobin, J. Biol. Chem. 277 (2002) 25783–25790.
[32] U. Samuni, D. Dantsker, A. Ray, J.B. Wittenberg, B.A. Wittenberg, S. Dewilde, L. Moens, Y. Ouellet, M. Guertin, J.M. Friedman, Kinetic modulation in carbonmonoxy derivatives of truncated hemoglobins. The role of distal heme pocket residues and extended apolar tunnel, J. Biol. Chem. 278 (2003) 27241–27250.
[33] D. Dantsker, C. Roche, U. Samuni, G. Blouin, J.S. Olson, J.M. Friedman, The position 68(E11) side chain in myoglobin regulates ligand capture, bond formation with heme iron, and internal movement into the Xe cavities, J. Biol. Chem. 280 (2005) 38740–38755.
[34] U. Samuni, C.J. Roche, D. Dantsker, L.J. Juszczak, J.M. Friedman, Modulation of reactivity and conformation within the t-quaternary state of human hemoglobin: the combined use of mutagenesis and sol–gel encapsulation, Biochemistry 45 (2006) 2820–2835.
[35] S. Bettati, A. Mozzarelli, T state hemoglobin binds oxygen noncooperatively with allosteric effects of protons, inositol hexaphosphate and chloride, J. Biol. Chem. 272 (1997) 32050–32055.
[36] P.J. Steinbach, Inferring lifetime distributions from kinetics by maximizing entropy using a bootstrapped model, J. Chem. Inf. Comput. Sci. 42 (2002) 1476–1478.
[37] P.J. Steinbach, R. Ionescu, C.R. Matthews, Analysis of kinetics using a hybrid maximum-entropy/nonlinear-least-squares method: application to protein folding, Biophys. J. 82 (2002) 2244–2255.
[38] S. Abbruzzetti, S. Bruno, S. Faggiano, L. Ronda, E. Grandi, A. Mozzarelli, C. Viappiani, Characterization of Ligand Migration Mechanisms Inside Haemoglobins from the Analysis of Geminate Rebinding Kinetics, Methods in Enzymology — Globins and Other NO-Reactive Proteins in Microbes, Plants and Invertebrates, 437, 2008, pp. 329–345.
[39] J.A. Hoy, H. Robinson, J.T. Trent, S. Kakar, B.J. Smagge, M.S. Hargrove, Plant hemoglobins: a molecular fossil record for the evolution of oxygen transport, J. Mol. Biol. 371 (2007) 168–179.
[40] M. Keil, T.E. Exner, J. Brickmann, Pattern recognition strategies for molecular surfaces: III. Binding site prediction with a neural network, J. Comput. Chem. 25 (2003) 779–789.
[41] T.A. Binkowski, S. Naghibzadeh, J. Liang, CASTp: computed atlas of surface topography of proteins, Nucleic Acids Res. 31 (2003) 3352–3355.
[42] A. Nicholls, K. Sharp, B. Honig, Protein folding and association: insights from the interfacial and thermodynamic properties of hydrocarbons, Proteins 11 (1991) 281–296.
[43] P.J. Goodford, A computational procedure for determining energetically favourable binding sites on biologically important macromolecules, J. Med. Chem. 28 (1985) 849–857.
[44] M.S. Hargrove, E.A. Brucker, B. Stec, G. Sarath, R. Arredondo-Peter, R.V. Klucas, J.S. Olson, G.N. Phillips Jr., Crystal structure of a nonsymbiotic plant hemoglobin, Structure 8 (2000) 1005–1014.
[45] E.E. Scott, Q.H. Gibson, J.S. Olson, Mapping the pathways for O2 entry into and exit from myoglobin, J. Biol. Chem. 276 (2001) 5177–5188.
[46] J.S. Olson, J. Soman, G.N. Phillips Jr., Ligand pathways in myoglobin: a review of Trp cavity mutations, IUBMB Life 59 (2007) 552–562.
[47] H.E. Harutyunyan, T.N. Safonova, I.P. Kuranova, A.N. Popov, A.V. Teplyakov, G.V. Obmolova, A.A. Rusakov, B.K. Vainshtein, G.G. Dodson, J.C. Wilson, M.F. Perutz, The structure of deoxy- and oxy-leghaemoglobin from lupin, J. Mol. Biol. 251 (1995) 104.
[48] A. Pesce, S. Dewilde, M. Nardini, L. Moens, P. Ascenzi, T. Hankeln, T.B. Bolognesi, Human brain neuroglobin structure reveals a distinct mode of controlling oxygen affinity, Structure 11 (2003) 1087–1095.
[49] M. Brunori, Q.H. Gibson, Cavities and packing defects in the structural dynamics of myoglobin, EMBO Rep. 2 (2001) 674–679.
[50] D. deSanctis, S. Dewilde, A. Pesce, L. Moens, P. Ascenzi, T. Hankeln, T. Burmester, M. Bolognesi, Crystal structure of cytoglobin: the fourth globin type discovered in man displays heme hexa-coordination, J. Mol. Biol. 336 (2004) 917–927.
[51] M. Lim, T.A. Jackson, P.A. Anfinrud, Nonexponential protein relaxation: dynamics of conformational change in myoglobin, Proc. Natl. Acad. Sci. U. S. A. 90 (1993) 5801–5804.
[52] L.P. Murray, J. Hofrichter, E.R. Henry, M. Ikeda-Saito, K. Kitagishi, T. Yonetani, W.A. Eaton, The effect of quaternary structure on the kinetics of conformational changes and nanosecond rebinding of carbon monoxide to hemoglobin, Proc. Natl. Acad. Sci. U. S. A. 85 (1988) 2151–2155.
[53] T. Hankeln, B. Ebner, C. Fuchs, F. Gerlach, M. Haberkamp, T.L. Laufs, A. Roesner, M. Schmidt, B. Weich, S. Wystub, S. Saaler-Reinhardt, S. Reuss, M. Bolognesi, D. DeSanctis,

M.C. Marden, L. Kiger, L. Moens, S. Dewilde, E. Nevo, A. Avivi, R.E. Weber, A. Fago, T. Burmester, Neuroglobin and cytoglobin in search of their role in the vertebrate globin family, J. Inorg. Biochem. 99 (2005) 110–119.
[54] J.S. Olson, G.N.J. Phillips, Kinetic pathways and barriers for ligand binding to myoglobin, J. Biol. Chem. 271 (1996) 17593–17596.
[55] K. Nienhaus, P. Palladino, G.U. Nienhaus, Structural dynamics of myoglobin: FTIR-TDS study of NO migration and binding, Biochemistry 47 (2008) 935–948.
[56] R.E.J. Brantley, S.J. Smerdon, A.J. Wilkinson, E.W. Singleton, J.S. Olson, The mechanism of autoxidation of myoglobin, J. Biol. Chem. 268 (1993) 6995–7010.
[57] E. Liong, Y. Dou, E. Scott, J. Olson, G. Phillips Jr., Waterproofing the heme pocket. Role of proximal amino acid side chains in preventing hemin loss from myoglobin, J. Biol. Chem. 276 (2001) 9093–9100.
[58] M. Brunori, Nitric oxide, cytochrome-*c* oxidase, and myoglobin, TIBS 26 (2001) 21–23.
[59] M. Brunori, Nitric oxide moves myoglobin centre stage, TIBS 26 (2001) 209–210.
[60] A. Bidon-Chanal, M.A. Martí, A. Crespo, M. Milani, M. Orozco, M. Bolognesi, F.J. Luque, D.A. Estrin, Ligand-induced dynamical regulation of NO conversion in *Mycobacterium tuberculosis* truncated-hemoglobin-N, Proteins 64 (2006) 457–464.
[61] M.A. Marti, A. Bidon-Chanal, A. Crespo, S.R. Yeh, V. Guallar, F.J. Luque, D.A. Estrin, Mechanism of product release in NO detoxification from *Mycobacterium tuberculosis* truncated hemoglobin N, J. Am. Chem. Soc. 130 (2008) 1688–1693.
[62] S. Abbruzzetti, S. Faggiano, S. Bruno, F. Spyrakis, A. Mozzarelli, S. Dewilde, L. Moens, C. Viappiani, Ligand migration through the internal hydrophobic cavities in human neuroglobin, Proc. Natl. Acad. Sci. U. S. A. 106 (2009) 18984–18989.